

Supporting Section:**Study of SERS Chemical Enhancement Factors Using Buffer
Layer Assisted Growth of Metal Nanoparticles on
Self-Assembled Monolayers**

Masato M. Maitani¹, Douglas A. A. Ohlberg³, Zhiyong Li^{3*}, David L. Allara^{1,2*},
Duncan R. Stewart^{3*}, R. Stanley Williams³

¹ Department of Materials Science and Engineering, The Pennsylvania State University,
University Park, PA 16802

² Department of Chemistry, The Pennsylvania State University, University Park, PA
16802

³ Information & Quantum Systems Laboratory, Hewlett-Packard Laboratories, 1501 Page
Mill Road, MS1123, Palo Alto, CA 94304, USA

S 1 Preparation of self-assembled monolayers and BLAG metal deposition

The procedure used to prepare the 1,4-benzenedithiol (BDT) SAM and 4-methylthiophenol (MBT) SAM on template stripped Au (TS-Au) surfaces is described in the previous paper.¹ The TS-Au surfaces used for all the experiments were supported on Si wafers using the method reported by Lee *et al.*² A 100 nm Au surface layer and 20 nm Ti barrier layer were deposited consecutively by electron beam evaporation at room temperature on a Si (001) template with a thermal oxide overlayer with a thickness of 20~40 nm. The Ti barrier layer served to prevent inter-diffusion between Au and the epoxy glue used in the stripping process. In the stripping process, the deposited Au/Ti layer on SiO₂ was glued to a Si handle wafer with thermally curable epoxy glue (Epoteck377, Epoxy Technology, Billerica, MA). After heating the sample to cure the glue at 150 °C for 8 hours, the Au surface was mechanically stripped off the SiO₂ template by wedging a razor blade between the handle wafer and template wafer. The TS-Au surface was then immediately immersed in a 0.1 mM solution of thiol in purified, anhydrous ethanol under a N₂ atmosphere at room temperature. Optimized immersion times for BDT and MBT were 1 h and 12 h, respectively. After immersion, the samples were rinsed with ethanol, dried under a N₂ flow, and loaded into an UHV chamber for BLAG deposition.

The metal deposition was performed in a home-built UHV chamber with a base pressure of 2×10^{-10} Torr. The Au was evaporated by a molybdenum boat thermal evaporator located 80 cm away from the sample surface. The deposition chamber contained a sample docking stage in thermal contact with a liquid He cryostat capable of cooling the stage to 10 K. The BLAG process can be briefly summarized as Xe buffer layer growth followed by metal deposition and subsequent Xe buffer layer sublimation. The process began with the initial cool-down of the sample stage (and mounted sample) down to 10 K. Xe gas was then introduced into the UHV chamber by a manually controlled needle valve to maintain a partial pressure of 2×10^{-6} Torr. The thickness of the condensed Xe buffer layer was calculated by assuming unitary sticking coefficients at Langmuir exposures ($L = \text{Torr} \cdot \text{s}$), as described in a previous report ($5.5 L = 1 \text{ ML}$ for Xe).³ The metal deposition rate was determined by a water-cooled quartz crystal monitor placed next to the sample stage. Temperature and pressure fluctuations of 0.5 K and $\sim 1 \times 10^{-8}$ Torr, respectively, were observed during the deposition of the metal. The applied voltage on the evaporation boat was adjusted to maintain a deposition rate of 1.0 Å / min. After metal deposition, a heater in the cryostat directed by a temperature control unit (Lakeshore 331, Lakeshore Cryotronics Inc., Westerville, OH) was used to slowly ramp the sample stage to a temperature plateau of 70 – 85 K to carefully insure that chamber pressures never exceeded 5×10^{-6} Torr during sublimation of the Xe. This was done in order to avoid perturbation of the deposited AuNps by abrupt pressure discharges that can result if the underlying Xe is allowed to sublime too rapidly. After the pressure dropped to $\sim 1 \times 10^{-9}$ Torr, the sample temperature was increased to room temperature (300K), and the sample was taken out of chamber. All analyses other than TEM imaging were performed at ambient conditions. The stability of the SAMs under UHV conditions were confirmed by RAIRS of control samples examined at each stage of the BLAG process up to the final metal deposition. At all stages no SAM desorption or degradation was observed.

S 2 Characterization of SAM on TS-Au

SAMs for reflection absorption infrared spectroscopy (RAIRS) and x-ray photoelectron spectroscopy (XPS) were prepared on a Au surface (~200 nm thick) thermally deposited on a Si wafer coated with a Cr (~70 nm) adhesion layer.^{1,4} SAMs on TS-Au substrates were used for the rest of characterization.

The thickness of the SAMs was measured by an ellipsometer (L117F300, Gaertner Scientific, Skoki, IL) with an incident angle and wave length of 70 degrees and 632.8 nm, respectively, for all samples after SAM preparation. The measured thickness of the BDT and MBT SAMs were 9.5 ± 1.3 Å and 8.8 ± 0.9 Å, respectively.

RAIRS of the BDT and MBT SAMs on Au were collected by a FT-IR spectrometer (FTS-7000, DigiLab, Randolph, MA) that was modified in-house with a customized optical setup.^{1,5} The liquid nitrogen-cooled, mercury-cadmium-telluride (MCT) detector had an effective low-frequency cutoff of ~ 750 cm^{-1} with a resolution of 2 cm^{-1} . The incident angle of the p-polarized IR beam was 86 degrees from the sample surface normal. To minimize the background interference in the spectral regions of interest for each sample, absorbance spectra, $-\log(R/R_0)$, were obtained using the SAM film of per-deuterated hexadecane thiolate ($\text{C}_{16}\text{D}_{33}\text{S}$) on Au as comparison blanks for the R_0 values¹. Peak assignments were based on previous reports and summarized in Table S2-1.⁶⁻⁸ Since the low frequency region contained artifacts caused by the cutoff of the MCT detector, our analysis of the spectra was focused on the high frequency region. The sharp intense peak at 1500 cm^{-1} is assigned to the in-plane, C-C stretching, 19a mode of the aromatic ring. This peak has a transition dipole moment parallel to the long molecular axis. The intense signals observed at 1500 cm^{-1} are indicative of near vertical oriented molecules. It was also determined from the strong similarity of the RAIRS spectra in the aromatic ring mode regions that there was not any significant orientational difference between the SAMs of BDT and MBT.

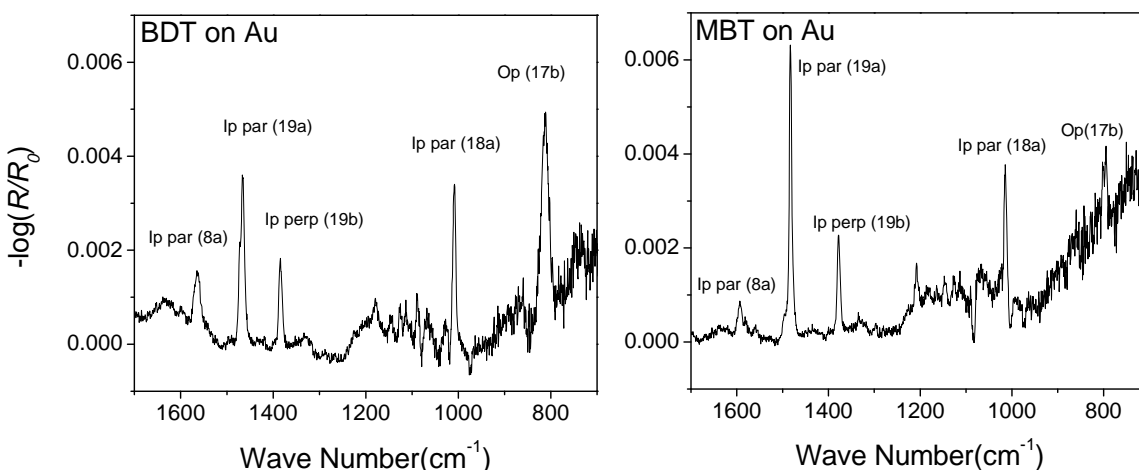


Figure S2-1. RAIRS of BDT SAM and MBT SAM on Au. Peaks are assigned with transition dipole moment; Ip par = in-plane parallel to molecular axis, Ip perp in-plane perpendicular to molecular axis, and Op = out-of-plane.⁶⁻⁸

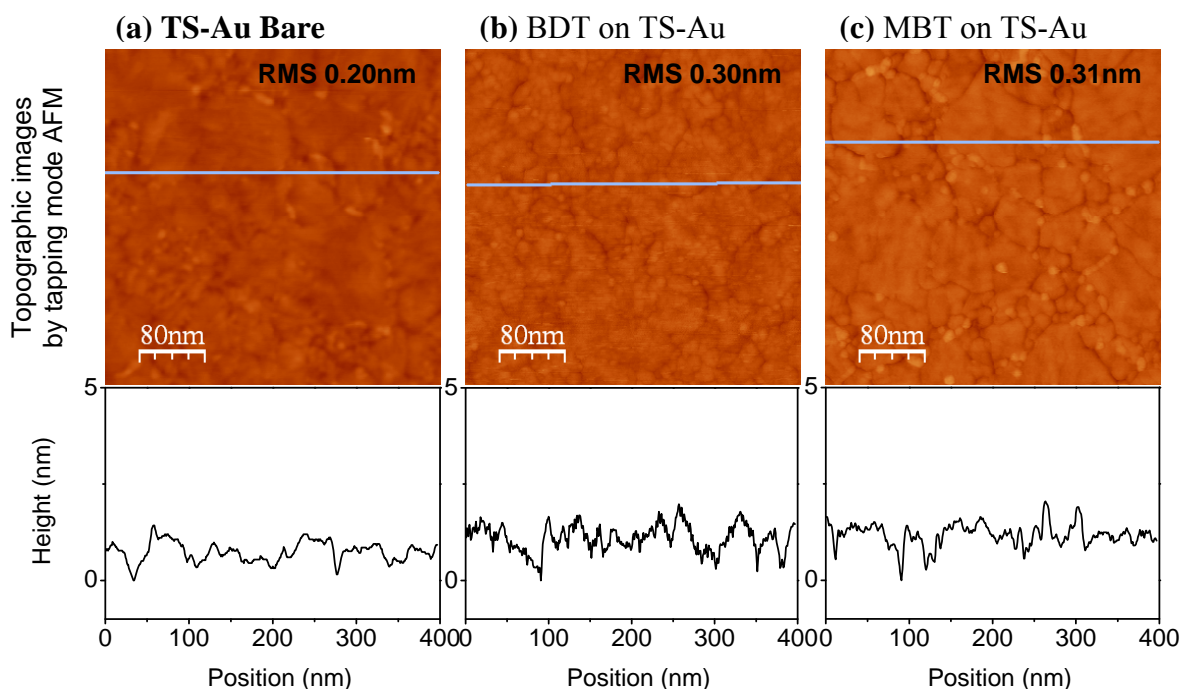


Figure S2-2. Topographic images and the corresponding line profiles of (a) TS-Au bare, (b) BDT SAM on TS-Au, and (c) MBT SAM on TS-Au surface taken by tapping mode AFM with the scan area of $0.4 \mu\text{m} \times 0.4 \mu\text{m}$.

Topographic images of the bare TS-Au, BDT SAM on TS-Au, and MBT SAM on TS-Au were taken with an AFM in tapping mode (Dimension 3100 Series with tapping mode Si tip (MPP-11100W), Veeco (Digital Instruments), Santa Barbara, CA) over a scan area of $0.4 \mu\text{m} \times 0.4 \mu\text{m}$. Topographic images with representative line scans of each surface are shown in figure S2-2. Slight change of surface from bare TS-Au substrates to the SAM-coated substrates with better resolved domain boundaries was observed, likely due to the reconstruction of Au surface by thiol molecules.² No significant difference was observed in the RMS roughness values and topography between BDT and MBT.

The XPS analyses were performed with a Kratos Analytical Axis Ultra (the monochromatic Al K_{α} source operated at an X-ray power of 280 watts, a take-off angle of 90 degrees with respect to the sample plane, a pass energy of 20 eV, and an energy step of 0.1 eV) under HV ($< \sim 5 \times 10^{-9}$ Torr). XPS spectra of the S2p region of the BDT and MBT SAMs on Au are shown in Figure S2-3. The S2p peaks were deconvoluted with a separation confinement and area ratio between the S2p_{1/2} and S2p_{3/2} components of 1.2eV and 2:1, respectively. The S2p components around 162eV were assigned to Au bonded sulfur and those at 163eV to the sulfur of free thiol or disulfide.⁸⁻¹⁰ The ratio between free thiol and bonded sulfur on the TS-Au substrate was 1.02:1. This ratio supports the conclusions that almost all BDT molecules in the SAM are free standing, and that the free thiol functional groups reside at the exposed SAM/ambient interface.

RAIRS, XPS, and ellipsometric thickness measurements all strongly support that both BDT and MBT molecules adopt the same structural orientation inside the SAM.

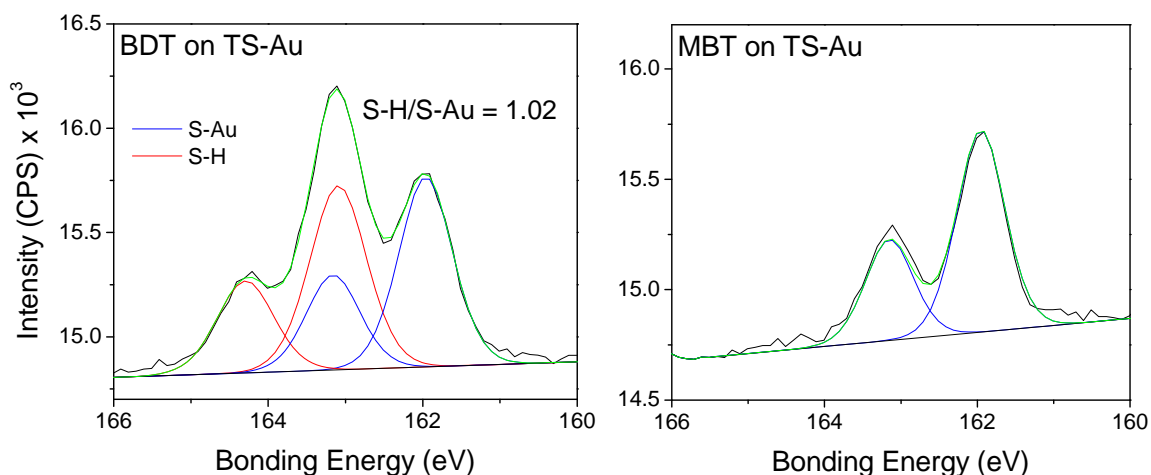


Figure S2-3 XPS of S2p core level of BDT and MBT SAM on Au showing Au bonded sulfur and free thiol. All spectra were referenced to the Au 4f_{7/2} at 84.0 eV. Plots with black, blue, red, and green indicate raw spectra, Au-bonded sulfur, sulfur of free thiol, and sum of deconvoluted peaks.

Raman spectra of SAMs on TS-Au (without AuNps), compound bulk samples of BDT and MBT, and AuNp-SAM-Au samples were taken with same the micro Raman spectrometer (JY-Horiba T6400, HORIBA Jobin Yvon Inc., Edison, NJ), equipped with a confocal microscope (OLYMPUS BX41, Olympus America Inc., Center Valley, PA), a liquid N₂ cooled CCD detector, and a HeNe laser (632.8 nm / 1 mW on a sample with D = 1 μm) as shown in Figure 2-4.

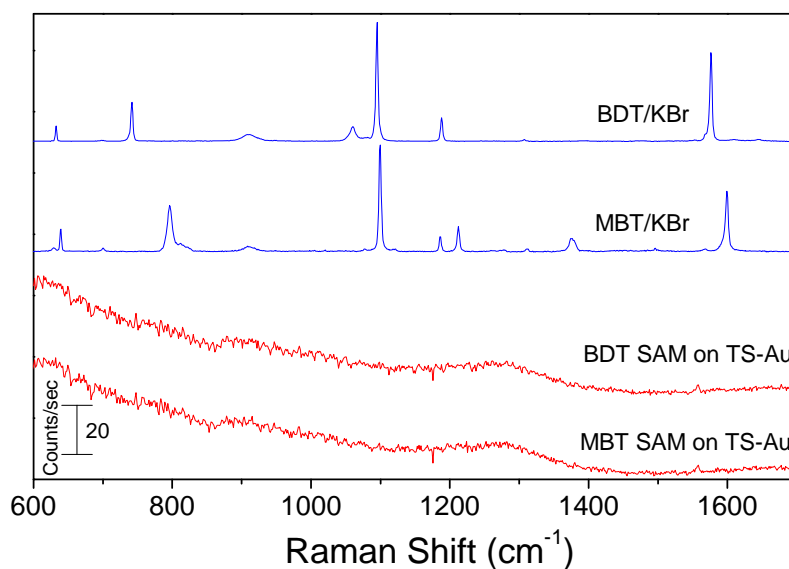


Figure S2-4. Raman spectra of BDT and MBT bulk and SAM on TS-Au without AuNp.

Table S2-1. Summary of peak assignment of RAIRS of SAM on Au (IRS), bulk Raman with KBr (BR), and SERS with AuNp-SAM-Au (SERS) spectra of BDT and MBT ^{a, 6-8}

BDT			MBT			Vibrational Assignment ^b		
IRS	BR	SERS	IRS	BR	SERS	Wilson Notion	Symmetry ^c	
							BDT	MBT
1564	1576	1557	1579	1599	1592	8a	A_g	A_1
	1553			1568		1555	8b	B_{3g}
1467	1478	1466	1484	1496		19a	B_{1u}	A_1
1385		1385				19b	B_{2u}	
			1378	1376		$\delta_s\text{CH}_3$		
	1307			1311		3	B_{3g}	B_2
	1267			1277		14	B_{2u}	B_2
			1208	1212		13		A_1
1178	1188	1179		1186		9a	A_g	A_1
	1095			1099	1079	1	A_g	A_1
	1065	1062				1	A_g	
1009		1008	1015			18a	B_{1u}	A_1
	910			909		$\beta(\text{SH})$		
813		813	794	796	816	17b	B_{3u}	B_2
	742	734				7a	A_g	
	698	696		700		4	B_{2g}	B_1
	632	637		639	623	6b	B_{3g}	B_2

^a Wave number in cm^{-1} . ^b Wilson notation. ^c Symmetry types corresponding to the D_{2h} and C_{2v} point group for BDT and MBT, respectively.

S 3 Analysis of AuNp-SAM-Au morphology

The size distribution of AuNps on BDT and MBT SAM for BLAG condition (I) was analyzed in detail from AFM images in Figure 2 in the main paper. Since the lateral size of AFM images is actually convoluted with AFM tip feature, therefore, we analyzed the size distribution of AuNps by their height. The height distributions for AuNP-BDT-Au and AuNP-MBT-Au prepared with BLAG condition (I), Au: 20Å / Xe: 150ML, resulting in uniformly distributed AuNps are plotted in Figure S3-1. Since the AFM tip cannot always access the Au substrate exposed between AuNps, we took the average of the lowest 200 points in each images from 512×512 points in 400×400 nm² as z positions representing Au substrate. The height of each AuNP was then derived from this global baseline for the scanned region. From this analysis, it is obvious that the AuNP size distribution on both BDT and MBT SAMs are almost same, with a mean size of $\sim 5 \pm 1$ nm.

Cross-sectional TEM images of AuNp-SAM-Au incorporating BDT and MBT SAMs prepared with BLAG condition (I) are shown in Figure S3-2. These images further reveal that AuNp morphologies on each of the SAMs are indistinguishable and appear to be in spherical shape.

From these two analyses, we conclude that AuNps on BDT and MBT SAMs do not show any observable morphological differences and therefore AuNps on two different SAMs contribute the same amplitude of EM enhancement in SERS spectra.

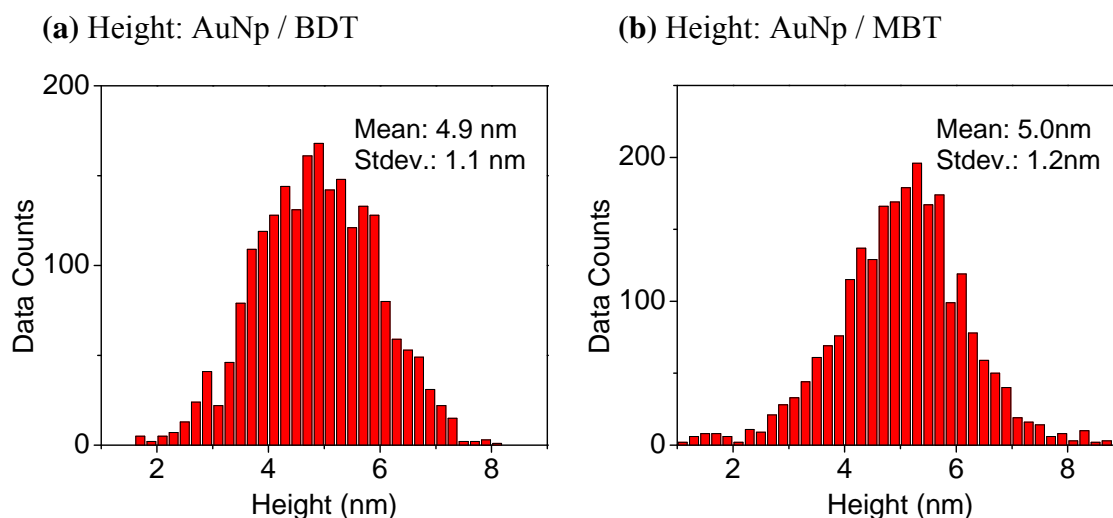


Figure S3-1. The height distribution of AuNp derived from AFM images (Figure 2 in the Communication) for (a) BDT and (b) MBT SAMs prepared with the BLAG condition (I) resulting in uniformly distributed AuNps.

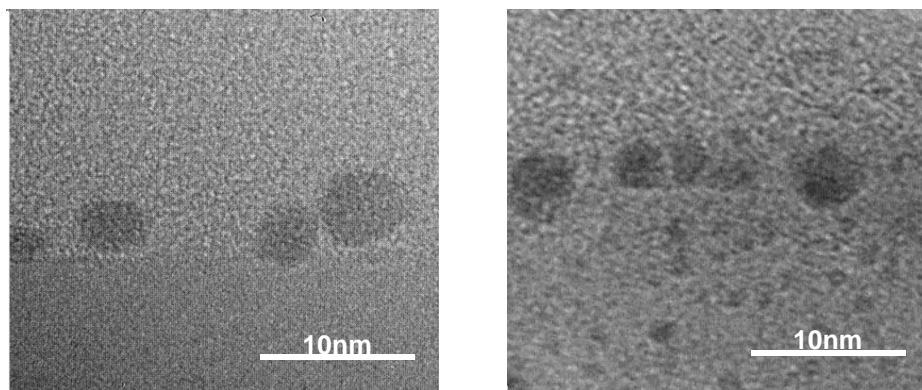


Figure S3-2. Cross-section TEM images of AuNp-SAM-Au incorporating (a) BDT and (b) MBT SAM prepared with the BLAG condition (I) resulting in uniform distribution. The white scale bars represent 10 nm distances.

S 4 4-Fluorobenzene thiol post-adsorption on AuNp-SAM-Au

Post-adsorption of 4-fluorobenzene thiol (FBT) onto AuNp-BDT-Au and AuNp-MBT-Au was performed by immersing each AuNp-SAM-Au samples prepared under BLAG condition (I) and (III) in 0.1 mM ethanol solution of FBT for 8 h and then rinsing thoroughly with ethanol to remove excess FBT. Control experiments with FBT adsorption on freshly evaporated gold substrates show from RAIRS measurements that a uniform SAM forms and ethanol rinsing does not remove the SAM. For reference, a Raman spectrum of pure FBT is shown in Figure S4 (right side). After the FBT treatment above neither the BDT nor MBT BLAG samples showed any spectral features expected for FBT, as illustrated in Figure S4 (left) for the case of BLAG condition (I) samples. The TEM data (Fig. S3-2) show that interparticle spacings are accessible nearly equally from the top and bottom (relative to the substrate plane), thus FBT molecules are expected to adsorb into these spacings from the top side upon exposure to an FBT solution. Since FBT has a Raman cross section comparable to MBT and BDT the lack of FBT Raman features in the treated BLAG samples suggests that the locations into which the FBT SAM adsorbs are not as enhancing as those associated with MBT and BDT between the Au substrate and the Au Np layers.

Based on the above, these control experiments suggest that the SERS spectra of MBT and DBT arise primarily from the molecules located in the AuNp-TS-Au substrate interface region as opposed to hot spots such as interparticle gaps where stray MBT or BDT molecules might migrate during the BLAG deposition or warm up processes. Furthermore, the control experiments also indicate that the BLAG AuNP-SAM-Au structure is a chemically stable system towards penetration by molecules from solution since no obvious thiol exchange with FBT was observed over 8 hours immersion in FBT solution. In contrast, extensive exchange is typically observed for such exposures of standard aromatic SAMs on planar gold substrates. Finally, the slight loss in intensity of the BDT peak after FBT immersion (Fig, S4) is ascribed to oxidative degradation of the thiolate groups in the BLAG samples which occurred from ambient exposure during the several week delay between BLAG deposition and FBT immersion experiments.

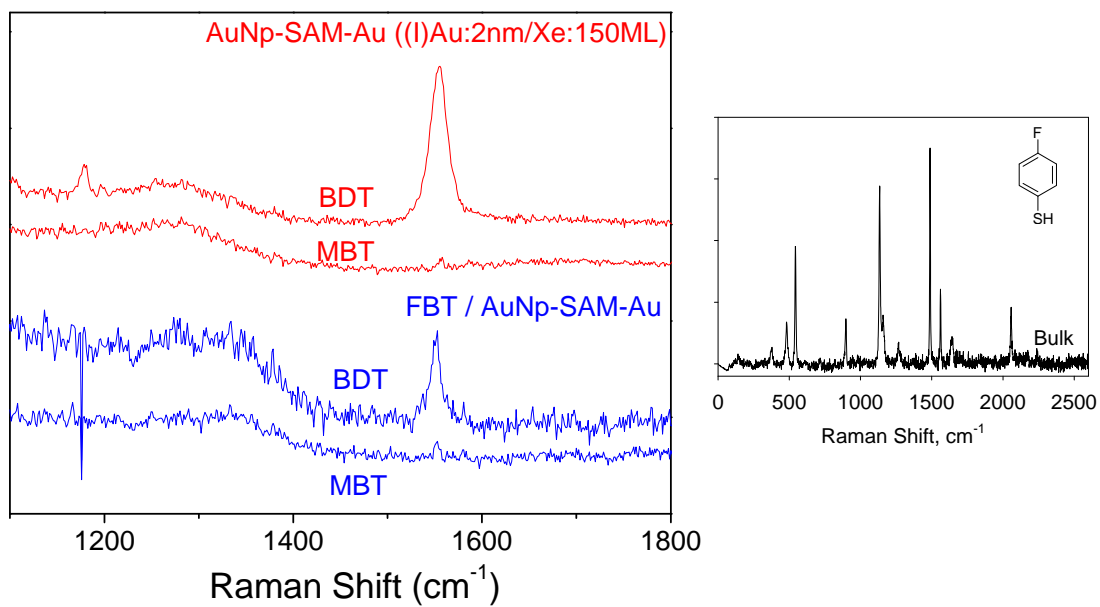
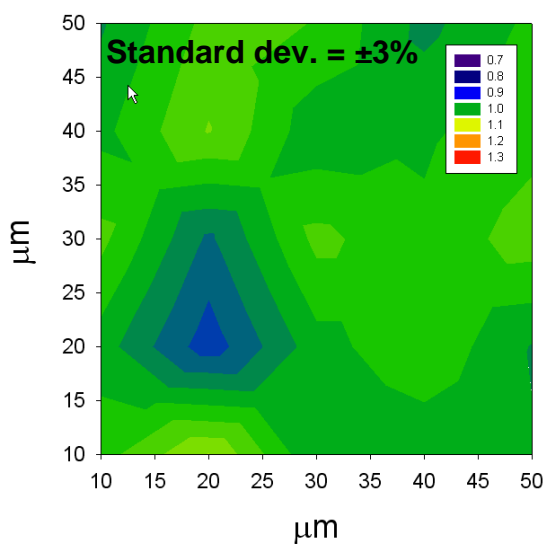


Figure S4. Raman spectra of AuNp-BDT-Au and AuNp-MBT-Au before and after FBT post-adsorption. A Raman spectrum of pure liquid FBT is shown on the right for reference.

S 5 Raman mapping on AuNp-SAM-Au

SERS intensity maps were collected for AuNp-BDT-Au surfaces prepared under the BLAG conditions of (a) Au: 20 Å / Xe: 150ML and (b) Au: 15 Å / Xe: 300ML \times 3cycles as shown in Figure S5. The intensity maps show the local intensity normalized over the average intensity of a 5×5 point sampling matrix across the surface with a spatial separation of $10 \mu\text{m}$ between points. The local SERS intensity was calculated as the integrated area of the spectral region from 1590 to 1510 cm^{-1} for both spectra. As expected from the AFM images, the uniformly distributed AuNp sample exhibited uniform spectral intensities across the surface. Multi-cycle deposition, on the other hand, resulted in a less uniform distribution of SERS intensity arising from the uneven distribution of AuNps with aggregated structures.^{11,12} For BLAG condition (I) (Au: 20Å / Xe: 150 ML), standard deviation of $< \sim 5\%$ within a sample area of $50 \times 50 \mu\text{m}^2$ was achieved, and $\sim 10\%$ within a sampled mm^2 region (data not shown).

(a) Au: 20Å / Xe: 150ML



(b) Au: 15Å / Xe: 300ML \times 3 cycles

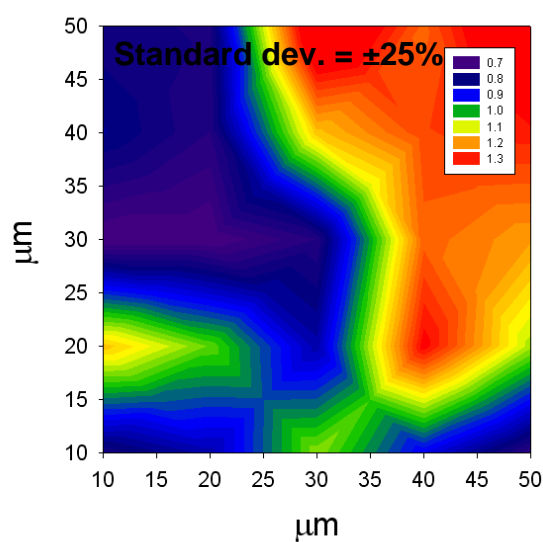


Figure S5. Map of relative intensity to the averaged intensity of 5×5 points across the surface with spacing of $10 \mu\text{m}$. BLAG conditions of AuNp-BDT-Au preparation are (a) Au: 20 Å / Xe: 150 ML and (b) Au: 15 Å / Xe: 300 ML \times 3 cycles.

S 6 Time dependant SERS of AuNp-SAM-Au

A water fall plot and corresponding SERS spectra of AuNp-BDT-Au was created using a 2 second integration interval with an incident beam of 633nm as shown in Figure S6. No blinking or degradation of the SERS spectra was observed within a few minutes of measurement, therefore, our AuNp-SAM-Au structure is stable enough to enable quantitative analysis under measurement conditions comparable to those of previously reported systems.¹³⁻¹⁶ This result may be another indication of how well the AuNps and TS-Au substrates sandwich structure stabilizes the BDT SAM through S-AuNp bonds and restricts any molecular movement or change of orientation.

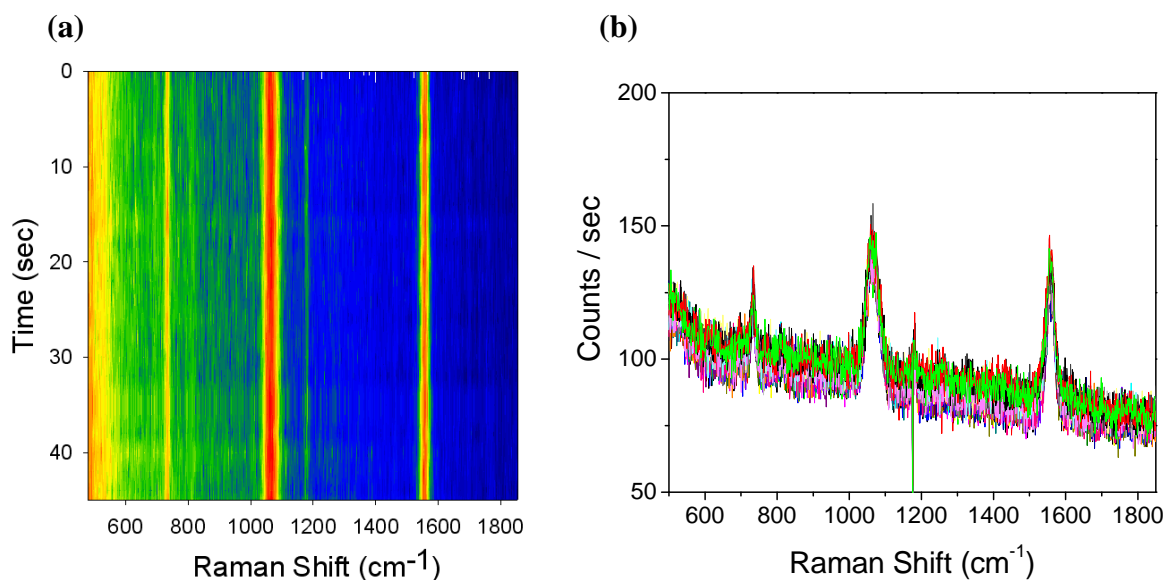


Figure S6. (a) A water fall plot and (b) corresponding SERS spectra of AuNp-BDT-Au obtained with 2 second integration with incident beam of 633 nm laser. BLAG condition is Au: 20 Å / Xe: 150 ML.

References

1. Nuzzo, R. G.; Dubois, L. H.; Allara, D. L. *J. Am. Chem. Soc.* **1990**, *112*, 558-569.
2. Lee, S.; Bae, S. S.; Medeiros-Ribeiro, G.; Blackstock, J. J.; Kim, S.; Stewart, D. R.; Ragan, R. *Langmuir* **2008**, *24*, 5984-5987.
3. (a) Haley, C.; Weaver, J. H. *Surf. Sci.* **2002**, *518*, 243-250. (b) Waddill, G. D.; Vitomirov, I. M.; Aldao, C. M.; Weaver, J. H. *Phys. Rev. Lett.* **1989**, *62*, 1568-1571. (c) Yoo, K., Li, A.-P., Zhang, Z., Weitering, H. H., Flack, F., Lagally, M.G., Wendelken, J.F. *Surf. Sci.* **2003**, *546*, L803-L807.
4. Konstadinidis, K.; Zhang, P.; Opila, R. L.; Allara, D. L. *Surf. Sci.* **1995**, *338*, 300-312.
5. Parikh, A. N.; Allara, D. L. *J. Chem. Phys.* **1992**, *96*, 927-945.
6. Varsanyi, G., *Assignments for Vibrational Spectra of Seven Hundred Benzene Derivatives*; John Wiley & Sons: New York, 1974.
7. Cho, S. H.; Han, H. S.; Jang, D. J.; Kim, K.; Kim, M. S. *J. Phys. Chem.* **1995**, *99*, 10594-10599.
8. Weckenmann, U.; Mittler, S.; Naumann, K.; Fischer, R. A. *Langmuir* **2002**, *18*, 5479-5486.
9. Esplandiu, M. J.; Noeske, P.-L. M. *Appl. Surf. Sci.* **2002**, *199*, 166-182.
10. Rieley, H.; Kendall, G. K.; Zemicael, F. W.; Smith, T. L.; Yang, S. *Langmuir* **1998**, *14*, 5147-5153.
11. Otto A. *J. Raman Spectrosc.* **2006**, *37*, 937-947.
12. Shalaev, V. M. *Physics Reports* **1996**, *272*, 61-137.
13. Constantino, C. J. L.; Lemma, T.; Antunes, P. A.; Aroca, R. *Anal. Chem.* **2001**, *73*, 3674-3678.
14. Krug, J. T.; Wang, G. D.; Emory, S. R.; Nie, S. *J. Am. Chem. Soc.* **1999**, *121*, 9208-9214.
15. Wang, Z.; Rothberg, L. J. *J. Phys. Chem. B* **2005**, *109*, 3387-3391.
16. Fromm, D. P.; Sundaramurthy, A.; Kinkhabwala, A.; Schuck, P. J.; Kino, G. S.; Moerner, W. E. *J. Chem. Phys.* **2006**, *124*, 061101-061104.